Natural Resources Canada | Ressources naturelles Canada

GEOLOGICAL SURVEY OF CANADA
OPEN FILE 9241

Enhanced seismicity monitoring in central Alberta, Canada: 2020–2022

J. Rojas-Parra, K.P. Marion, R.O. Salvage, and D.W. Eaton

2025

Canada

GEOLOGICAL SURVEY OF CANADA
OPEN FILE 9241

Enhanced seismicity monitoring in central Alberta, Canada: 2020–2022

J. Rojas-Parra[1], K.P. Marion[1], R.O. Salvage[1,2], and D.W. Eaton[1]

[1]Department of Earth, Energy and Environment, University of Calgary, 2500 University Drive N.W., Calgary, Alberta T2N 1N4
[2]Natural Resources Canada, Geological Survey of Canada, 3303-33 Street N.W., Calgary, Alberta T2L 2A7

2025

This publication is available for free download through the NRCan Open Science and Technology Repository (https://ostrnrcan-dostrncan.canada.ca/).

Recommended citation
Rojas-Parra, J., Marion, K.P., Salvage, R.O., and Eaton, D.W., 2025. Enhanced seismicity monitoring in central Alberta, Canada: 2020-2022; Geological Survey of Canada, Open File 2941, 1 .zip file. https://doi.org/10.4095/pps3fqydpq

Publications in this series have not been edited; they are released as submitted by the author.

ISSN 2816-7155
ISBN 978-0-660-76579-2
Catalogue No. M183-2/9241E-PDF
https://doi.org/10.4095/pps3fqydpq

Executive Summary

Efforts to move towards a net-zero target of carbon emissions, require that new technologies be developed to address energy demand. One such technology is represented by closed-loop geothermal systems, whereby fluid is circulated through a network of deep interconnected wellbores to heat the fluid. These systems, also known as Advanced Geothermal Systems (AGS), are designed such that the circulating fluid does not enter the in-situ pore space. They can be operated in a broad range of geothermal gradients and geological settings. Much like a radiator, AGS systems utilize passive heat conduction through long lateral wells, eliminating the need to fracture the reservoir. Conventional and enhanced geothermal systems (EGS), by comparison, involve injection and/or exchange of fluids directly in the subsurface, and therefore into pore spaces, which has the potential to induce seismicity.

This study set out to directly test the potential for induced microseismicity brought about through the operation of a closed-loop AGS prototype installed by Eavor Technologies Inc. (Eavor) in Clearwater County, Alberta. This AGS system was originally proposed, permitted, and installed by Eavor in late 2019. The University of Calgary, working in partnership with Eavor, installed four passive broadband seismometers within 10 km of the closed-loop geothermal system from November 2020 to November 2022. This publication is intended to facilitate the public dissemination of results from this study, including a documentation of methodologies and interpretations, which may foster continued research into closed-loop geothermal development in Canada.

Analysis of the continuous seismic data, including the detection of potential seismic events, their locations and magnitudes was undertaken by the University of Calgary and the Geological Survey of Canada using a machine learning approach, with data from the four temporary local stations, as well as the public seismic network within a radius of 350 km (10 additional stations), covering much of west central Alberta and southeastern British Columbia. Event origin times from available seismic catalogs were also used. With this approach, 94 seismic events in the study region were identified, with magnitudes ranging from M_L 0.94 to M_L 4.09. Phase picks were manually inspected, and hypocentre locations were determined using a probabilistic nonlinear global-search algorithm. Events within the new catalog included quarry blasts, natural seismicity (e.g. 14 February 2021 Banff earthquake) and events located within well-documented seismicity clusters (e.g. south-west of Rocky Mountain House). No events were detected within the footprint of the installed monitoring array, or within the area surrounding the closed-loop AGS prototype, to a distance of ~25km. Although the estimated magnitude of completeness of the determined catalog is M_L 2.24, events proximal to dense station coverage as small as M_L 0.94 were detected. The lack of any detected seismic activity within ~25km of the 4-station EVR array around the closed-loop geothermal system provides a high level of confidence that no events with $M_L > 1$ were induced by operations during the two-year monitoring period.

Introduction

Seismicity in Western Canada (Alberta and British Columbia) has been attributed to natural causes related to far-field tectonic stress, as well as to more local stress perturbations, including changes in pore pressure associated with resource exploration and development practices such as hydraulic fracturing, saltwater disposal and enhanced oil recovery (e.g. Atkinson et al., 2016; Horner et al., 1994; Rivard et al., 2014, Salvage et al., 2024). Seismic events that have a causal link to any human activity are known as induced events. Unlike other parts of Canada, most of Alberta is considered tectonically quiescent and lacks a history of significant seismicity (Lamontagne et al., 2008; Milne et al., 1978; Natural Resources Canada, 2015; Stern et al., 2013). The relative stability of this region has been attributed to its intraplate tectonic setting, which contrasts with patterns of seismicity in plate boundary settings, which are relatively fixed in space and periodic in nature. Seismic hazard in Alberta may be impacted by extensive faulting and fracturing related to the formation of the Rocky Mountains (e.g., Rebollar et al., 1984; Ross et al., 1991). When natural earthquakes do occur, these earthquakes are typically small ($M_L < 4$) and spatially associated with basement faults or thrust faults in the Cordillera (e.g. on the eastern flank of the Rocky Mountains, following the southeast-trending foreland belt; Stern et al., 2013).

Seismicity inferred to be induced by natural gas production has been observed in central Alberta, southwest of Rocky Mountain House, since the 1980's (Wetmiller, 1986). Beginning in 2013, additional seismic monitoring stations near Red Deer, within the province's public Regional Alberta Observatory for Earthquake Studies Network (RAVEN) network (Alberta Geological Survey, 2013), have been installed for surveillance of induced seismicity in this area; however, the network station density is insufficient to achieve a magnitude of completeness of M_L 1.0. Instead, the required level of monitoring (as set out by Provincial legislation) must be achieved by industry-operated private networks. Data acquired using these private networks is not generally available to the public or for research purposes.

The present study focuses on the East Shale Basin of Alberta's Duvernay Formation, from the city of Red Deer to the edge of the Rocky Mountain deformation front and stretching as far south as Calgary (113° to 117.5°W and 51° to 53.5°N). The Duvernay East Shale Basin is in early stages of development as an unconventional resource play and has potential for tight oil production in west central Alberta (Thorson et al., 2019).

A widely felt M_L 4.6 (local magnitude) earthquake near Sylvan Lake, west of Red Deer, on 4 March 2019 confirms that this region has seismogenic potential that is comparable to the Fox Creek region of Alberta (Natural Resources Canada, 2019), where induced seismicity has been observed since 2013 (e.g. Schultz et al., 2017). Due to the evident risk of induced seismicity, on December 9, 2019, through Subsurface Order 7, the Alberta Energy Regulator (AER) established a regional traffic light protocol (TLP) for Duvernay well completions, as well as an exclusion zone around the Dickson Dam and its reservoir (Gleniffer Lake). A TLP is a regulatory framework that provides response provisions within a region of industrial development, such as hydraulic fracturing or geothermal exploration. The Red Deer TLP has stricter constraints on seismic activity than the TLP imposed on the Kaybob region near Fox Creek (Subsurface Order 2) in northwestern Alberta due to the increased risk associated with operations close to the city of

Red Deer. Within the area covered by Subsurface Order 7, the magnitudes for yellow- and red-light thresholds, which impose preventive measures or a halt in operations, respectively, are M_L 1 and M_L 3. By comparison, the yellow and red magnitude thresholds in the (more remote) Kaybob-Duvernay region covered by Subsurface Order 2 are M_L 2 and M_L 4.

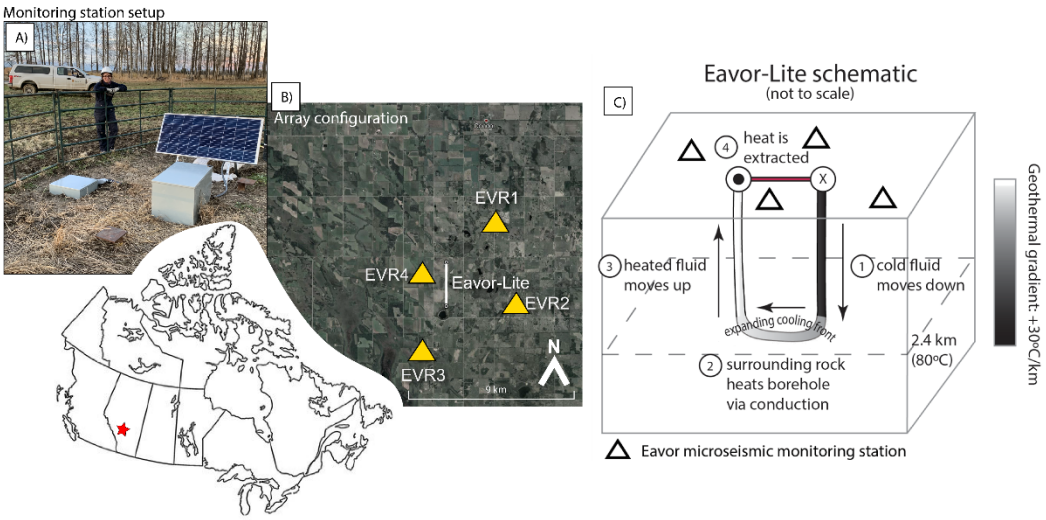

Figure 1: A) Equipment configuration at station EVR4. Stations were powered by 12V batteries connected to a solar panel. B) Location of the four monitoring stations (yellow triangles) installed for this study, with their station names (EVR1-4). The location of the study area is shown by the red star in the overview map of Canada. C) Simplified diagram of the Eavor-Lite™ closed-loop geothermal system, adapted from Eavor (2020).

In late 2019, Eavor Technologies Inc. (Eavor) established the Eavor-Lite™ demonstration project, an advanced geothermal system (AGS) in the municipality of Clearwater County in west-central Alberta (Figure 1). The surrounding region encompasses the town of Rocky Mountain House and the traditional territories of the O'Chiese and Sunchild Cree First Nations. Eavor-Lite™ is a closed loop system and, in principle, does not produce any increase in fluid pressure within the geothermal reservoir zone. However, it has been suggested that thermoelastic stress changes due to cooling of the surrounding rock mass could cause stress changes that are sufficient to trigger seismicity (e.gPerkins and Gonzalez, 1985; Candela et al., 2018). The closest public monitoring seismometer to the Eavor-Lite™ project is greater than 30 km away, and thus with the existing network the magnitude detection threshold and hypocentral location accuracy, especially in terms of earthquake focal depth, are not optimal at the site. As such, a local seismic monitoring network of four broadband sensors (Table 1) around the Eavor-Lite™ demonstration project, herein referred to as the EVR array, was installed by the University of Calgary, in collaboration with Eavor, in November 2020, and operational until November 2022 to monitor potential microseismicity in the area (Figures 1 and 2). The data from the EVR array were gathered with the following objectives:

1. To provide enhanced coverage of the Eavor-Lite™ geothermal operation to confirm if any detected events are linked to the geothermal operations;

2. If microseismicity is detected, to provide a feasibility test of whether an array of surface seismometers could be used to track the thermal front within the geothermal reservoir through thermoelastic effects, and;
3. To provide enhanced coverage of induced seismicity within the Duvernay East Shale basin for academic research.

The Eavor-Lite™ system (Figure 1C) consists of two intersecting horizontal wells drilled into a low-permeability sandstone unit at 2.4 km depth, where the reservoir temperature is ~78°C. The well geometry creates two "legs" that are connected and sealed (Vany et al., 2020). Fluid moves via a thermosiphon effect down the cold wellbore, through the loop legs capturing heat from the surrounding rock via conduction, before returning to the surface passively (Eavor, 2020; Toews, 2021). Eavor-Lite™ began operation in December 2019. The horizontal wellbores are oriented north-south in an area where the reservoir unit has an average thickness of 15 m and dips gently to the west (Toews et al., 2020; Vany et al., 2020). A local stress model shows that at the reservoir depth S_{hmin} (minimum horizontal stress; 16-18 kPa/m) < S_V (vertical stress; 23-24 kPa/m) < S_{hmax} (maximum horizontal stress; 28-30 kPa/m), where S_{hmax} has an azimuth between 30 ° to 60° (Vany et al., 2020). This represents a strike-slip faulting regime, consistent with regional stress maps (Reiter and Heidbach, 2014), and shows that S_{Hmax} is oriented approximately perpendicular to the Rocky Mountain deformation front. Toews (2021) reported the Eavor-Lite™ facility runs at 95% uptime with minimal leak-off rates (< 0.5 m^3/day), suggesting that fluid exchange with the reservoir is negligible.

In addition to data collected for this project using the four installed stations that comprise the EVR array (Network Code: EO), data from publicly available seismic stations (Table 1) were used to construct a seismicity catalog between November 2020 and November 2022. Data for the public stations (1 November 2020 – 30 November 2022, Network Codes: CN, RV, TD) were downloaded directly from the global archive services provided by the Seismological Facility for the Advancement of Geoscience (SAGE; www.iris.edu). Some stations within the study area either provided incomplete or unusable data (e.g. due

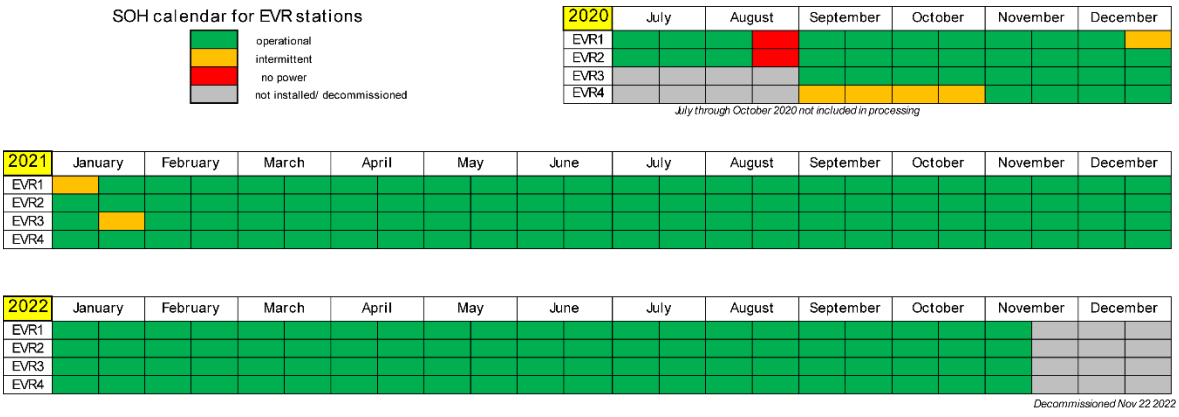

Figure 2: State of health (SOH) calendar for the EVR array. There were no known issues after February 2021, such that the dataset provides 2 full years of coverage. Green suggests the station was fully operational; yellow indicates intermittent data collection; red indicates no data collected and grey indicates that the station was not operational (i.e. not installed or decommissioned).

to low signal to noise) and were therefore omitted from the study (unlabelled stations in Figure 3). Collectively, the data from the stations enabled earthquake activity (natural or induced) to be characterized throughout a broad region of central Alberta around the EVR array, encompassing the breadth of west-central Alberta (Figure 3).

Regional seismicity close to the EVR array

No historical seismicity ($M_L > 2.0$) has been reported by the AER within 20 km of the Eavor-Lite™ system (Alberta Energy Regulator, 2023; Figure 3). However, west-central Alberta and southeastern British Columbia encompasses several previously known seismicity clusters that have been described individually in the literature: the Duvernay East Shale Basin (Figure 3, close to RD; Hui et al., 2021; Wang et al., 2020), the Fox Creek area (Figure 3, close to station EGLEA; Schultz et al., 2017, Wang et al., 2016), seismicity close to Peace River (Figure 3, close to PR; Vasyura-Bathke et al., 2023; Schultz et al., 2023), and the Rocky Mountain House Seismogenic Zone (Figure 3, close to RMH; Baranova et al., 1999; Rebollar et al., 1982, 1984; Wetmiller, 1986).

Methodology

Station installation, monitoring and maintenance

Four temporary seismic stations (EVR1 - EVR4) were installed between July and September 2020 by the University of Calgary, within 5 km of the Eavor-Lite™ wells. The stations were located on rural properties in Clearwater County, which overlapped with existing oil and gas leases for abandoned or low-volume gas wells (Figure S1, Table S1). Each station was monitored for state of health using a cellular uplink to ensure operational quality over the two-year monitoring period (Figure 2). Regular field visits were initially necessary since each seismometer was powered by three 12-volt batteries that needed periodic charging. The power systems were upgraded in November 2020 when solar panels were retrofitted to each station, after which nearly continuous data were acquired. In mid-December 2021, the GPS arm of EVR1 was damaged (likely by an animal), causing the station to appear offline as it could not reach the cellular network. However, the station continued recording until the next service visit when the GPS arm was repaired. Several sensors appeared to go off-centre due to ground tilting during each spring thaw, but this was fixed remotely over the cellular uplink. Data were last harvested on November 24, 2022, and the sites were fully reclaimed in August 2023, when the digitizer housing was removed.

Data harvesting

Since the EVR sites were relatively remote and had poor cellular reception, streaming large volumes of data in real-time was not feasible. Thus, regular visits to download the data were necessary. Data were converted to miniseed format from Nanometrics STOR files (Nanometrics Inc., 2012) for ease of analysis.

Station and channel metadata (RESP and Station XML files) were then created. All data were backed up to portable external hard drives, and continuous waveform data, as well as associated metadata for EVR1 – EVR4, are available on the SAGE facility at https://doi.org/10.7914/SN/EO, following an embargo period until 25 November 2024.

Network Code	Station Code	Latitude [degrees]	Longitude [degrees]
CN	EDM	53.223	-113.3497
EO	EVR1	52.277951	-114.54776
EO	EVR2	52.238691	-114.5315
EO	EVR3	52.214748	-114.60465
EO	EVR4	52.253068	-114.60843
TD	TD002	53.4394	-114.387642
TD	TD008	52.804089	-115.431763
TD	TD009	52.32058	-116.32337
TD	TD022	51.17701	-114.228798
RV	YELLA	53.23671	-117.14084
RV	REDDA	52.179264	-113.90344
RV	BELVA	49.587654	-114.377174
RV	MKRVA	49.143002	-111.775467
RV	EGLEA	54.457111	-116.440483

Table 1: Seismic stations used in this study. Stations EVR1-EVR4, representing the EVR array, were installed by the University of Calgary as part of this study.

Public and Private sources of data

Multiple external sources of data including additional public seismic stations (Figure 3, Table 1) were used to provide the most complete earthquake catalog possible for west central Alberta. Open access data from the Seismological Facility for the Advancement of Geoscience (SAGE) were downloaded via the ObsPy open-source software (Beyreuther et al., 2010; Krischer et al., 2015), using the MassDownloader function.

This included the RAVEN network (Regional Alberta Observatory for Earthquake Studies Network; Schultz and Stern, 2015) operated by the Alberta Geological Survey, and the TD Network operated by Nanometrics. Stations that provided data for only part of the investigation time were omitted to better constrain the magnitude of completeness of the catalog, which can be affected by changes in station distribution. A regional catalog of seismicity generated by the Alberta Energy Regulator (AER), accessible through the online Earthquake Dashboard (https://ags-aer.shinyapps.io/Seismicity_waveform_app/), as well as access to a private catalog of events generated for Alberta using private TD stations (herein named the TA catalog), provided a useful comparison for our catalog in terms of event detection, location and magnitude

Data processing

A machine-learning based workflow was used to process all continuous seismic data. The workflow entailed four main steps:

1. Event detection and phase picking
2. Phase association
3. Hypocentre location
4. Magnitude estimation

Combining the seismicity catalog generated using the EVR array data and a machine learning approach with origin times from existing seismicity catalogs available from the AER and TD networks allowed the generation of a more complete catalog. As part of this process, phase arrivals were carefully re-examined and re-picked for every potential event from any available catalog. Events with insufficient high-quality phase picks were removed, and hypocentre locations obtained using a consistent method (grid-search algorithm) and velocity model were computed. As such, hypocentre locations were re-computed using manual phase picks as part of this study, rather than taking reported locations from either the AER catalog or the TA catalog.

Event detection and phase picking

For purposes of preliminary event detection and initial phase picking, the advanced neural network-based automatic picking method PhaseNet (Zhu and Beroza, 2018) was used. This approach has been found to outperform traditional methods like short-term average/long-term average (STA/LTA) pickers with respect to processing speed and improved event sensitivity (Chai et al., 2020). STA/LTA methods compare the ratio of desired seismic signal to noise over a sliding time window until a trigger value is exceeded (Trnkoczy, 2009). PhaseNet is a pre-trained neural network – using real picks made by human interpreters for training – that outputs P-wave and S-wave arrival times for waveforms from three component seismometer data as probability distributions (Zhu and Beroza, 2018). Arrival cutoffs are determined using a user-defined probability threshold. Arrival times are measured from the peak of the distribution and are

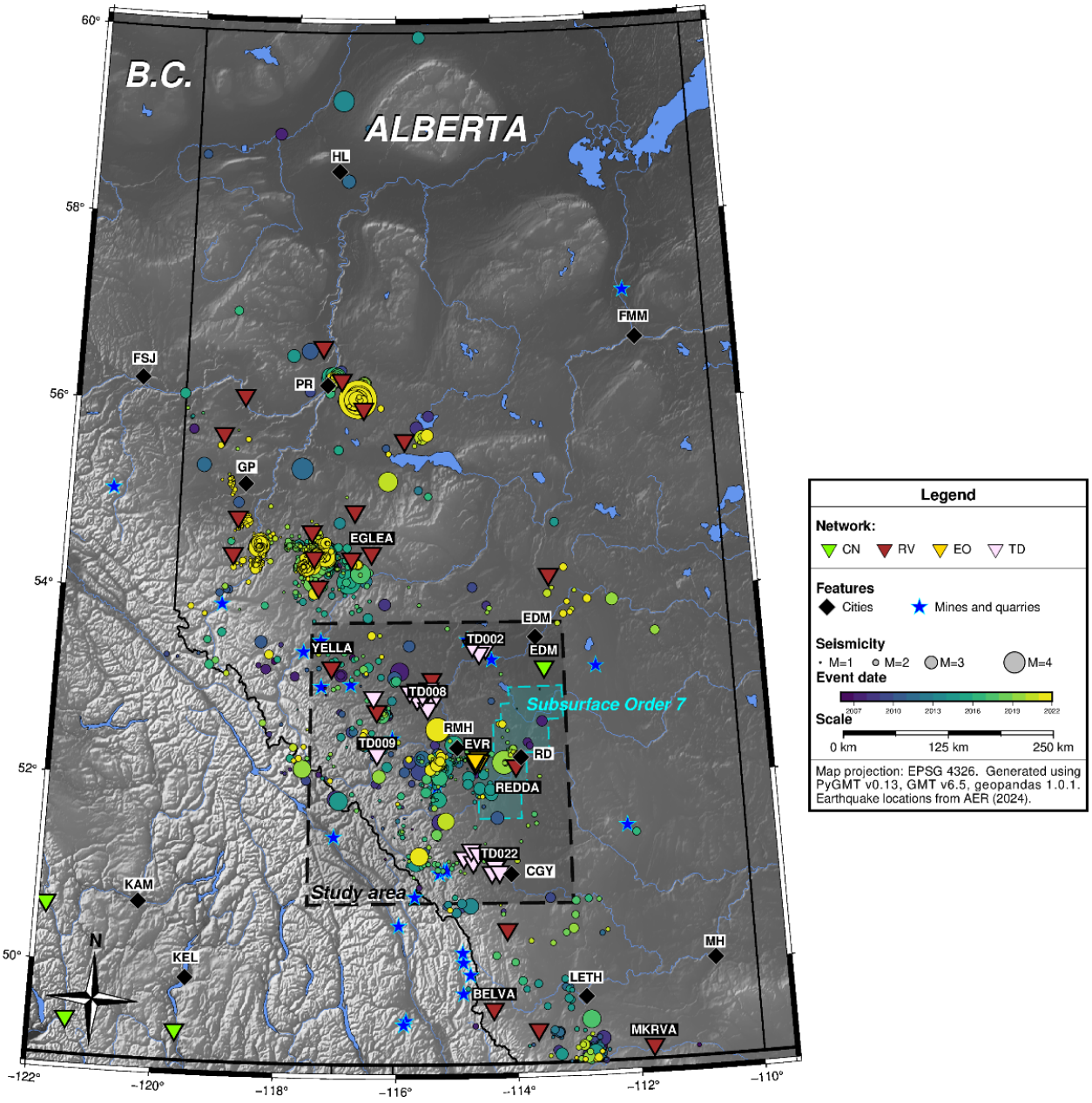

Figure 3: Map of seismic monitoring stations (inverted triangles) in Alberta and eastern British Columbia, showing the primary study area (black dashed line), which encompasses west-central Alberta and parts of southeastern British Columbia. Stations used in this analysis are labelled by name; those not used (due to incomplete data or high signal to noise) are not labelled. Mines and quarries are indicated by blue stars. Settlements are shown as black diamonds: High Level (HL); Fort McMurray (FMM); Peace River (PR); Fort St. John (FSJ); Grand Prairie (GP); Edmonton (EDM); Red Deer (RD); Rocky Mountain House (RMH); Calgary (CGY); Kamloops (KM); Kelowna (KEL); Medicine Hat (MH); Lethbridge (LETH). Seismicity, coloured by time from 2016 to 2022 and scaled by magnitude, from the Alberta Geological Survey catalog (https://ags-aer.shinyapps.io/Seismicity_waveform_app/) are shown as circles.

not threshold dependent, unlike STA/LTA pickers. As such, this detection algorithm can also be run without prefiltering the data, saving time and computational effort. The PhaseNet model has been successfully applied to various seismic monitoring datasets both in its default state and following re-training, providing

improved performance (Chai et al., 2020, Li et al., 2024). For new datasets, shortfalls of this approach include reduced thresholds of pick probability level determined by the software, relative to datasets that are more consistent with the original training datasets, which may result in an increased number of false positive detections. Therefore, all phase picks obtained using this approach were manually inspected.

Phase association

Phase detection over the 2-year investigation period using PhaseNet generated > 100,000 phase detections, which required a subsequent phase association step to group phase picks into potential events. The GaMMA (Gaussian Mixture Model Associator) package (Zhu et al., 2022) approaches this problem by treating phase association as an unsupervised clustering problem, wherein earthquake phases follow a hyperbolic moveout of phase travel times from the origin of the event. Event detections require calibration to locally tuned velocity models at both regional and local scales. GaMMA utilizes DBSCAN (Ester et al., 1996, Schubert et al., 2017), a density-based clustering algorithm, which can be applied to clusters regardless of shape, noise, or outliers and without knowledge of the number of clusters. Earthquake source parameters such as the location and origin time are determined in a matter of minutes by GaMMA using the Expectation Maximization algorithm, avoiding the time-consuming and computationally expensive alternative of grid-search algorithms.

In the spirit of generating as many potential events for review as possible, 5 different iterations of GaMMA were used to generate a list of potential earthquake events (Table S2). GaMMA requires a single value for P- and S-wave velocity (Vp and Vs, respectively), because of the hyperbolic moveout applied to phase arrivals. As the study area is relatively large, three different velocity scenarios were applied to the continuous dataset; derived from the velocity model used by Schultz et al. (2023) and applying a weighted average (by layer thickness) to it (Table 2).

Experimenting with increasing the maximum phase time residual (s, max_sigma1) from 2.5 to 15 seconds had a large impact on the apparent conversion rate of seismic events (oversample vs. mid; Table S2). Varying the epsilon value (dbscan_eps), a DBSCAN parameter that describes the radius of the neighborhood that still includes a minimum number of core points (i.e., whether the point belongs to a cluster or is considered noise), from 30 to 60 seconds did not have a large impact on the number of detected events. Increasing the number of initial earthquake locations (cluster centers) by varying the initial points from [1, 1, 1] for (x,y,z) directions to [2, 2, 1] was suggested as an improvement for large areas by Zhu et al. (2022). However, this did not significantly impact the total number of detected events (Table S2).

Event location

To determine earthquake hypocentre locations based on the output from PhaseNet and GaMMA, NonLinLoc was used (Lomax et al., 2014; Lomax et al., 2000), a probabilistic, non-linear, global-search earthquake location algorithm. Modified forms of the layered velocity model from Schultz et al. (2023), as shown in Table 2 were tested. NonLinLoc uses a nonlinear probabilistic global-search approach along with

Depth [km)	Layer thickness [km]	Vp [km/s]	Vs [km/s]	Density [g/cm^3]
0.0	0.4	2.50	1.00	1.4
0.4	0.4	3.03	1.31	1.6
0.8	0.4	3.56	1.62	1.7
1.2	0.4	4.10	1.92	1.9
1.6	0.4	4.63	2.23	2.4
2.0	0.2	5.16	2.54	2.6
2.2	0.8	6.00	3.50	2.7
3.0	2	6.00	3.50	2.7
5.0	2	6.10	3.55	2.7
7.0	2	6.20	3.60	2.7
9.0	2	6.30	3.65	2.7
11	15	6.40	3.70	2.7
	Weighted average	**6.08**	**3.49**	

Table 2: Velocity model used in this study, adapted from Schultz et al. (2023).

a least-squares objective function to assess the best-fitting hypocentre location for an event. The difference between observed and predicted phase arrival times (i.e., the residual) is minimized at each monitoring station. Input parameters for NonLinLoc are shown in Table S3. The output of this algorithm includes relocated hypocentre coordinates (including depth) and their associated positional uncertainties (see Supplementary Data) for any potential event identified through this machine learning workflow.

Magnitude estimation

For magnitude determination, the method of Babaie-Mahani and Kao (2020) was used, who proposed a local magnitude scale for the Western Canada Sedimentary Basin based on observations from British Columbia. As a first step for magnitude calculation, the instrument response function for a station needs to be removed, to convert the raw data into units of displacement (in m). Next, the Richter local magnitude scale is considered,

$$M_l = log(A) - log(A_o) + S,$$

where A is the recorded amplitude, in millimeters on a Wood-Anderson seismograph, A_0 is the distance correction term and S is a correction term for each station that takes care of systematic amplitude changes such as local site effects. For this calculation, the Wood-Anderson response was convolved with the waveforms to generate magnitude calculations. For the distance correction, the inferred values are

$$-log(A_o) = \begin{cases} 0.671 \times log(\frac{R_{hypo}}{100}) + K & : R_{hypo} \leq 85km \\ -0.881 \times log(\frac{R_{hypo}}{100}) + K & : R_{hypo} > 85km \end{cases},$$

where K is defined as

$$K = 0.003 \times (R_{hypo} - 100) + 3.0.$$

Consistent with Babaie-Mahani and Kao (2020), only the vertical component of the seismic recordings was used to calculate magnitude, after applying the instrument response correction. The S term was not determined for each individual station; instead, the median of all the amplitudes per event was used.

Following the approach outlined above, a consistent difference of ~0.79 magnitude units was observed between the local magnitude (M_L) for events that were determined using the machine learning approach compared with the same events from the AER online catalog (https://ags-aer.shinyapps.io/Seismicity_waveform_app/).. This discrepancy likely reflects systematic differences between the methodology used for magnitude calculation, however, the exact details of the AER magnitude calculation are not known. Nevertheless, the consistency of the magnitude difference provides strong assurance that the magnitudes are valid in a relative sense. In order to maintain consistency with the AER reported catalog, which for this region provides a regulatory reference catalog, a constant value of 0.79 magnitude units was added to all of the computed magnitudes in the machine learning catalog, since it was not feasible to calculate magnitudes using the AER magnitude calculation.

Catalog compilation and refinement

After implementation of the workflow described above, a preliminary event catalog covering the period from 1 November 2020 to 30 November 2022 was created, which included any event detected using the machine learning workflow (Table S2; a total of 230 unique events within the study area). To further supplement the catalog, we included any event identified in either the AER earthquake catalog (95 unique events) or an event identified in a private catalog provided to the University of Calgary produced by Nanometrics Ltd. and TransAlta (denoted as the TA catalog; a total of 1583 unique events). This preliminary catalog containing all events was used to extract 1-minute data windows for potential events that started at the catalog event origin times. After data extraction, events were manually inspected and phases manually picked/readjusted on all available stations, and then re-located using the same velocity model (Table 2) and a standardized procedure (NonLinLoc with parameters as Table S3) to ensure catalog completeness. Most events within the TA catalog were disregarded since significant errors were found in their locations (mis-location by several hundred kilometers) by analysis of S-P phase arrival times. The final combined catalog contains 94 unique events and is provided with this report as supplementary files in CSV and QuakeML format. The QuakeML file includes phase pick times.

All events in the AER catalog within the study area were also present in the TA catalog and the machine learning generated catalog, and most of the events in the TA catalog that were not in the AER catalog were detected in the preliminary catalog generated by the machine learning workflow. Manual picking of P and S arrivals was performed for every event using the Snuffler open-source software package(https://pyrocko.org/docs/current/apps/snuffler/manual.html). Figures 4 and 5 show examples of

events with manually picked phases obtained using Snuffler. The combined machine learning catalog identified an additional 60 unique events within the study area between November 2020 and November 2022, compared to the AER catalog.

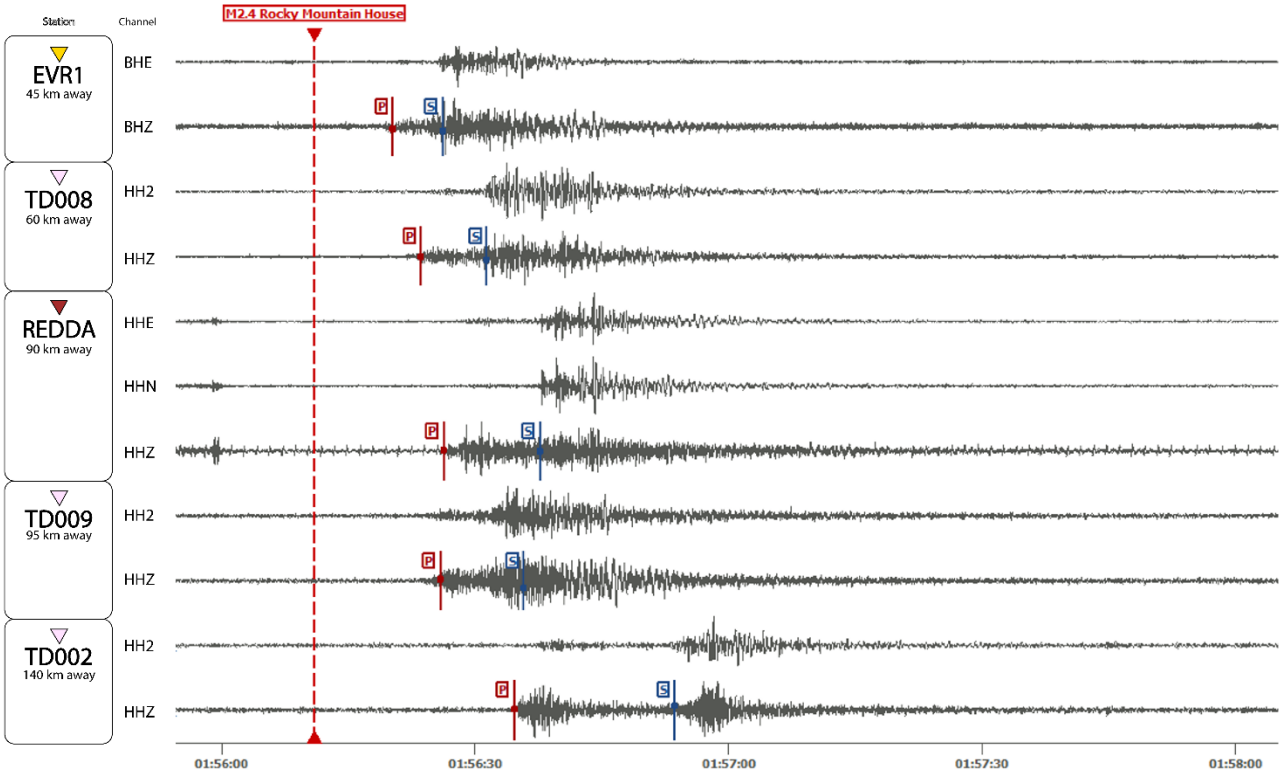

Figure 4: Example waveforms for a M_L 2.4 seismic event located 53 km from the array on 6 September 2022 at 01:56:12 UTC, showing manual phase picks obtained using Snuffler. Each line in the plot represents a different station and component (shown on the left). The red vertical dashed line shows the interpreted event origin time; solid read vertical lines represent picked P-phases; solid blue vertical lines represent picked S-phases. Both phase picks are shown on the Z (vertical) component, for comparison.

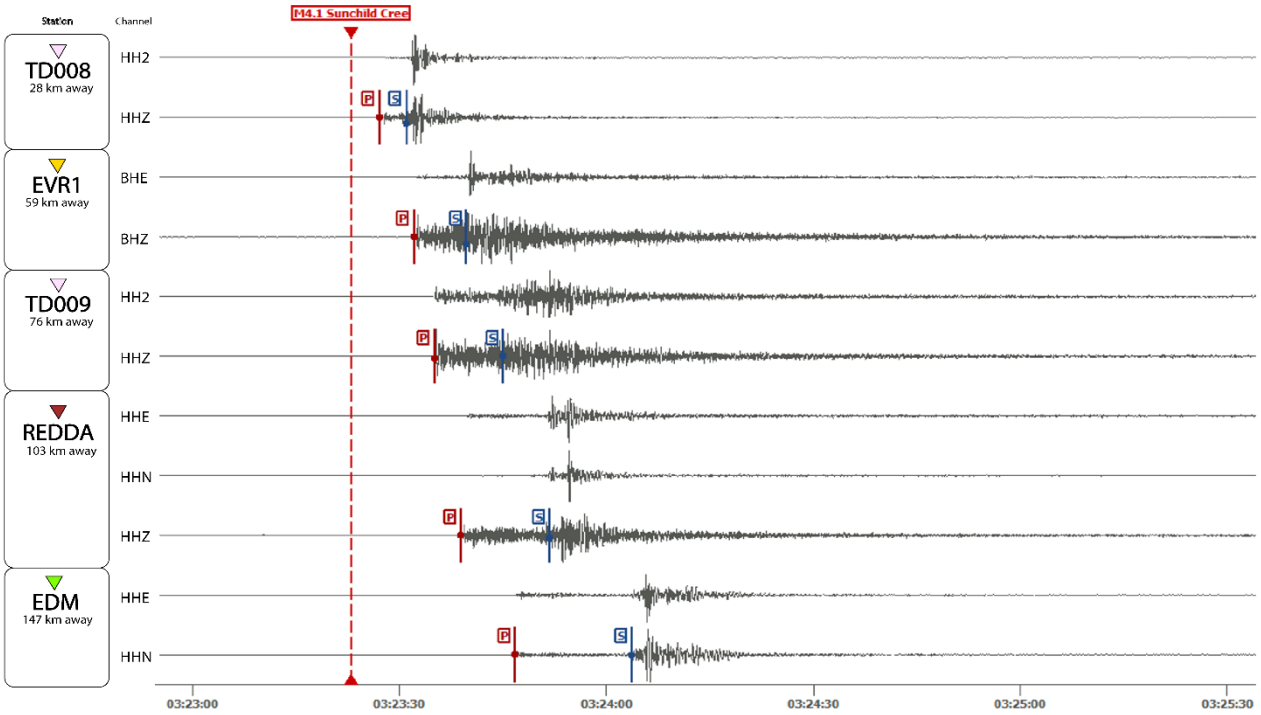

Figure 5: Example of the M_L 4.1 Sunchild Cree event located 60 km from the array on 21 October 2021 at 03:23:22 UTC, showing manual phase picks obtained using Snuffler. Each line in the plot represents a different station and component (shown on the left). The red vertical dashed line shows the interpreted event origin time; solid read vertical lines represent picked P-phases; solid blue vertical lines represent picked S-phases. Both phase picks are shown on the Z (vertical) component, for comparison.

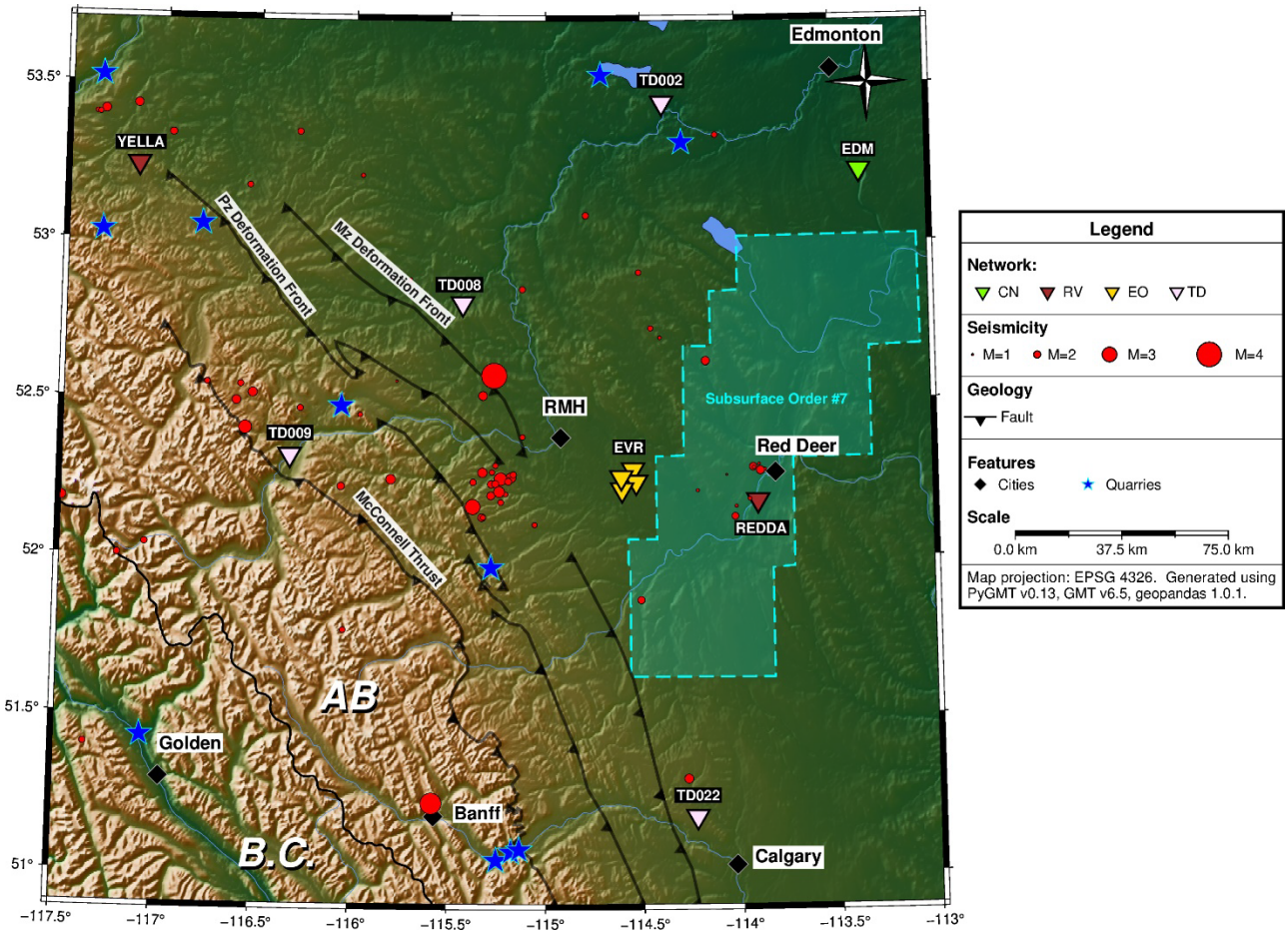

Figure 6: Map of the study area, showing the 94 events from the machine learning derived catalog (red circles), with diameter proportional to calculated local magnitude. Cities and towns are depicted as black diamonds (RMH = Rocky Mountain House); seismic stations are depicted as inverted triangles, with colour indicating the respective network; Quarries are shown as blue stars. The Rocky Mountain fold-and-thrust belt is demarcated by several thrust faults orientated NW-SE. The TLP area defined by Subsurface Order #7 is marked with the green shaded polygon. Fault locations were provided courtesy of geoLOGIC systems © 2024.

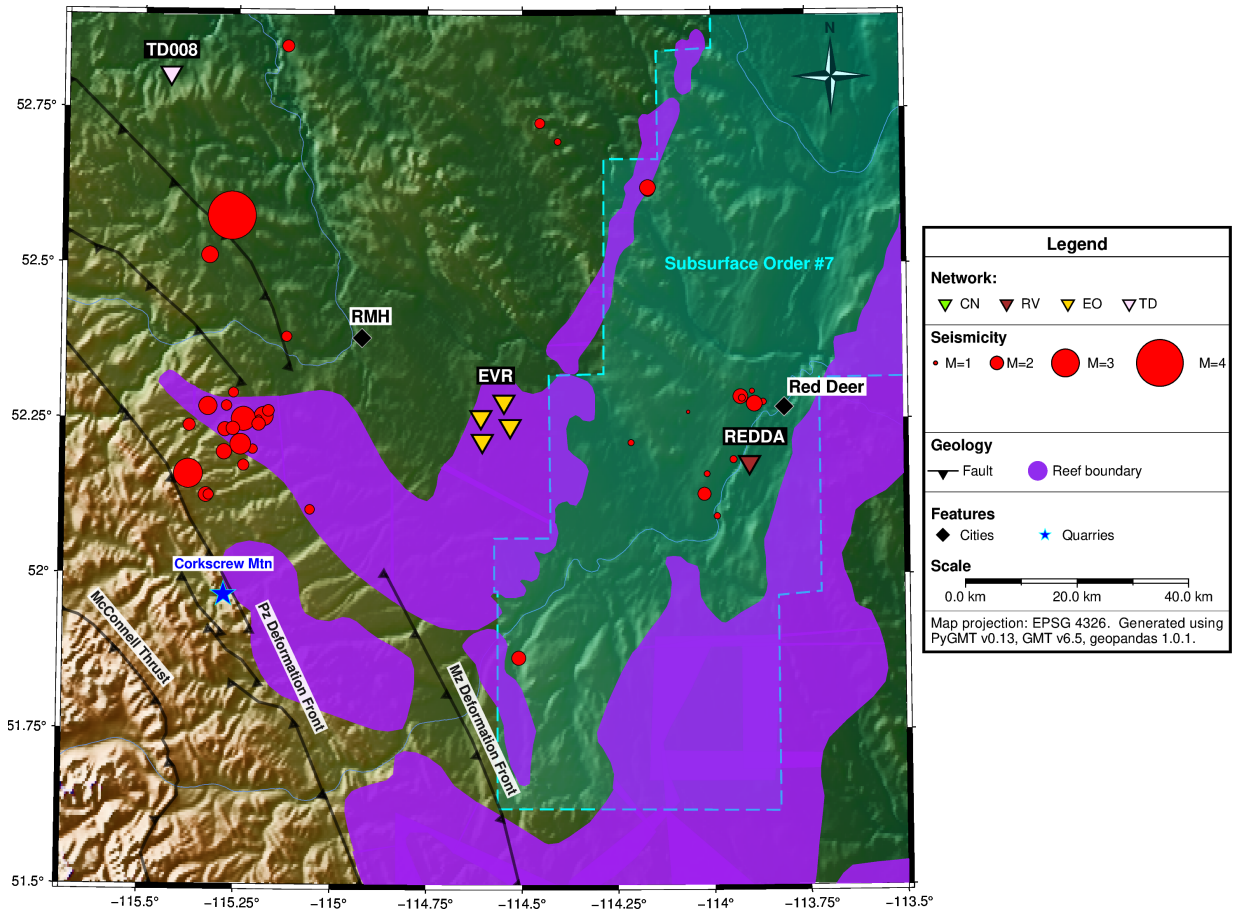

Figure 7. Enlarged map of the region surrounding the EVR monitoring array (yellow inverted triangles), with the events detected in this study shown as red circles with diameter proportional to calculated local magnitude. Settlements are depicted as black diamonds (RMH = Rocky Mountain House); seismic stations are depicted as inverted triangles, with colour denoting the network; Quarries are shown as blue stars. Major geological features such as the Leduc reef boundary (purple shading) are shown, along with several thrust faults orientated NW-SE. The reef boundary is shown because it has been proposed that proximity to Leduc-reef boundaries constitutes a risk factor for induced seismicity (Schultz et al., 2016). Fault polygons and Leduc Reef outline (purple) were provided courtesy of geoLOGIC systems © 2024.

Results

After careful review of every potential event detection from both the five iterations of the machine learning catalog plus re-picking and re-locating events identified in the AER catalog and/or the TA catalog, a total of 94 events were confirmed and located within the study area (Figures 6 and 7), using the methodology described above for the period from November 2020 to November 2022. Potential events that were ruled out by visual inspection included teleseismic events, clearly evident blasts at nearby quarries, as well as regional earthquakes near Fox Creek and other parts of Alberta that occurred outside the study area. The remaining seismicity is sparsely distributed (Figure 6). In the final catalog, magnitudes range from M_L 0.94 to M_L 4.08, which represents both very small local events and regional felt events. Focal depths range from near surface (~0.01 km) to 10 km deep, although depth error estimates indicate a high degree of uncertainty in this parameter with a minimum depth error of ~1.75km (see seismicity catalog in Supplementary Data). This large uncertainty is likely due to the sparse station locations across such an extensive region.

The Gutenberg-Richter law expresses the nearly universal relationship between the event magnitudes and total number of earthquakes in a given region and time period (Gutenberg and Richter, 1944). It can be written as

$$\log N = a - bM \; ; \;\; M > M_c$$

where a and b are fitted empirical parameter, and N is the number of events in the catalog with magnitude greater than or equal to M, and M_c is the magnitude of completeness (i.e. the magnitude above which the catalog is deemed to be complete; Eaton, 2018). Figure 8 shows an empirical magnitude-recurrence graph computed based on the final catalog of 94 events, along with predicted falloff in magnitude based on the Gutenberg-Richter relationship with various representative values of the b-parameter. M_c is estimated here to be 2.24 using the method of Wiemer and Wyss (2000), although the majority of events detected actually sit below this magnitude of completeness. This further highlights that, although the seismic array was capable of detecting small magnitude events located close to stations, the sparse overall station distribution resulted in a higher value of M_c across the study area.

Blasting

Numerous mines and quarries are active in west-central Alberta, and it is therefore important to differentiate blasting from natural seismic activity. Blast sites are fixed in space and regulated, and certain waveform characteristics (i.e., emergent onset, ringy waveform characteristics, relatively strong surface waves) can be easily identified in the data. Moreover, blasts typically occur at nearly the same time-of-day, during the daytime shift. Events suspected to be blasts have been identified within the catalog but have not been removed, for the sake of completeness, however, known blasting events have been removed

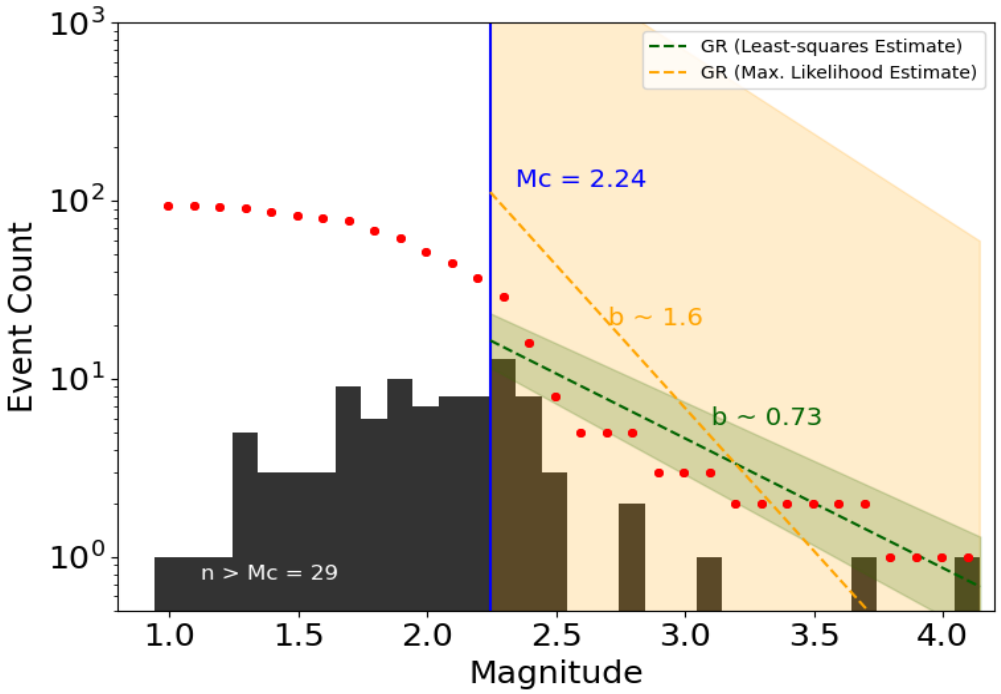

Figure 8: Magnitude-frequency distribution for the seismicity catalog presented in this study. The estimated magnitude of completeness (Mc) is 2.24 using the method of Wiemer and Wyss (2000), although it is clear from the distribution that many detected events are smaller than this. This likely reflects a sparse and irregular throughout the study region. 29 events in the catalog were estimated to have magnitudes above the M_c. Two estimated *b*-values are presented: a linear least squared regression estimate (green; *b*~0.73), and the maximum likelihood estimate of Aki (1965; yellow, *b*~1.6).

Rocky Mountain House Seismogenic Zone (RMHSZ)

The cluster of seismicity south-west of Rocky Mountain House (Figures 6 and 7) has been active since at least 1976 and continued to be seismically active during the monitoring period. It is interesting that seismicity has persisted, as gas production was thought to be the primary causal mechanism for the seismic activity, although gas production has ceased. The cause of such activity is therefore debated but could relate to nearby saltwater disposal (Eaton and Eyre, 2018; Marion et al., 2023). In general, of the closest events to the EVR array in the final catalog lie within this region.

Detection of natural events

Fortuitously for this study, two of the largest recorded natural earthquakes in Alberta's history were well recorded by the array, presenting a unique opportunity for further study of their origin. As discussed below, both events were well detected by the local EVR array.

Sunchild Cree event: October 21, 2021, M_L 4.1

The largest event recorded by the EVR array occurred on October 21, 2021, at 03:23:22 UTC (Natural Resources Canada, 2021a) near the Sunchild Cree 202 reserve, at a calculated depth of 7.6 km and located approximately 60 km NW of the EVR array. In Figure 7, this event is evident at a location that is approximately midway from RMH (Rocky Mountain House) to station TD008. This is one of the largest earthquakes to occur in the province in the past 50 years. Comparison with the provincial catalog suggests a cluster of seismicity that is geographically distinct from the Rocky Mountain House Seismogenic Zone may exist in this area; Figure 9 presents another example of an event in the same area that likely belongs to this group. As this cluster is proximal to the home of the Sunchild Cree peoples, we refer to this group of seismicity as the Sunchild Cree cluster.

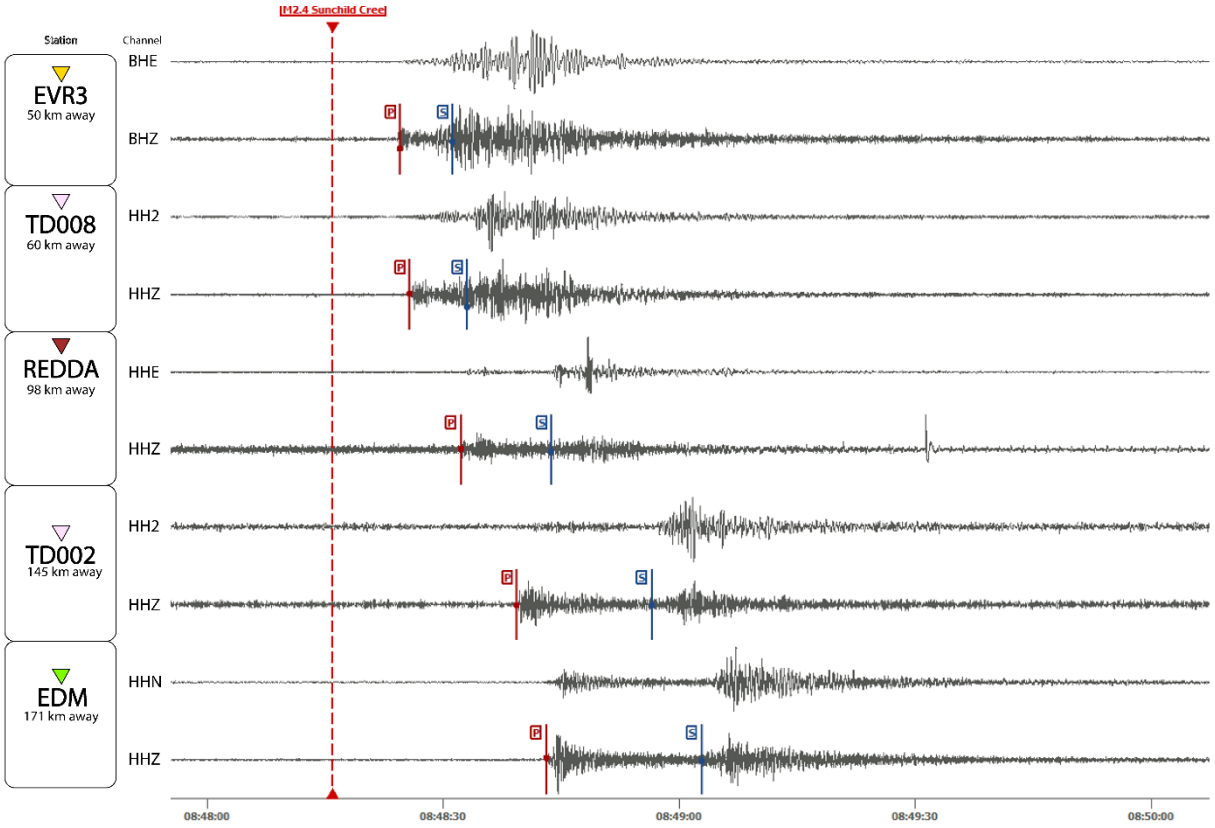

Figure 9: A M_L 2.3 event from 22 December 2021 at 08:48:15 UTC that is suspected to belong to the same cluster as the M_L 4.1 event shown in Figure 5, showing manual phase picks using Snuffler. Each line in the plot represents a different station and component (shown on the left). The red vertical dashed line shows the interpreted event origin time; solid read vertical lines represent picked P-phases; solid blue vertical lines represent picked S-phases. Both phase picks are shown on the Z (vertical) component, for comparison.

Banff event: February 14, 2021, M_L 3.66

A second significant event occurred on February 14, 2021, at 01:33:10 UTC, ~135 km SW of the EVR array (Natural Resources Canada, 2021b; Figure 10). It was lightly felt in the municipalities of Banff,

Canmore and Sparwood. The calculated depth of the event (~1.5 km deep) places it within an area of Cenozoic faulting (Gabrielse and Yorath, 1991), however previous estimates for the event depth (5 km; Natural Resources Canada, 2021b) places it well below any Laramide thrust faults in the area and implies that the hypocentre lies within crystalline basement, possibly at the edge of the Rimbey magmatic arc (e.g. Brown and Spang, 1978).

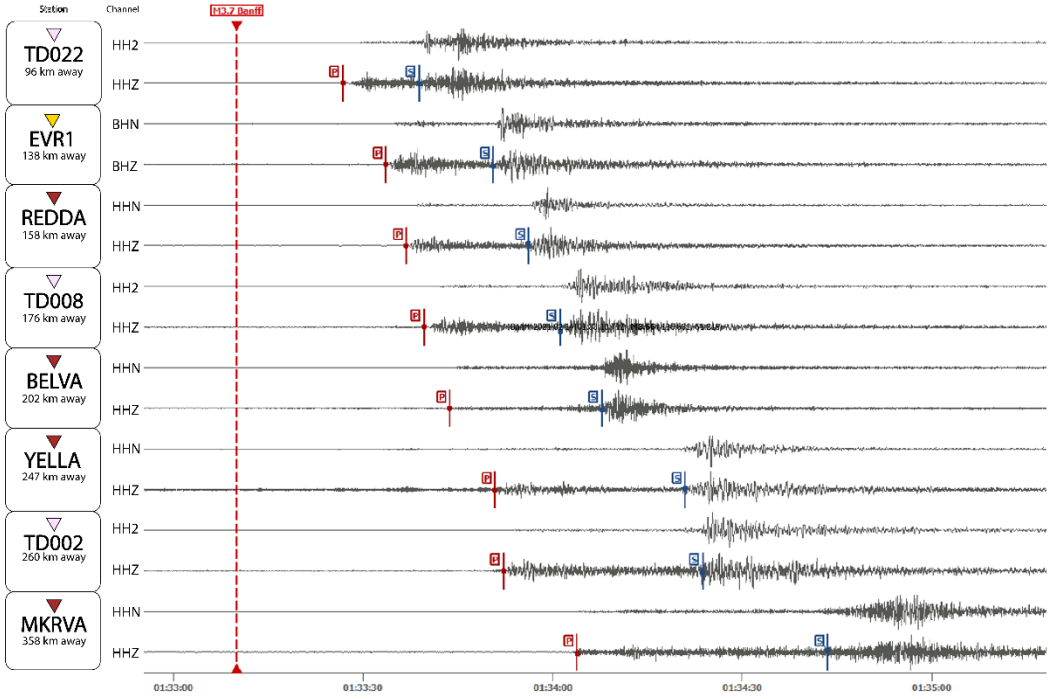

Figure 10: The second largest event in the seismicity catalog is a M_L 3.66 event near Banff, located ~135 km away from the EVR array, which occurred on 14 February 2021 at 01:33:10 UTC. Each line in the plot represents a different station and component (shown on the left). The red vertical dashed line shows the interpreted event origin time; solid read vertical lines represent picked P-phases; solid blue vertical lines represent picked S-phases. Both phase picks are shown on the Z (vertical) component.

Absence of seismicity proximal to the Eavor-Lite™ system

As evident from the seismicity catalog (Supplementary Data) and from the event distribution (Figures 6 and 7), no events were detected in this study within 25 km of the Eavor-Lite™ system. The observation of events in the final catalog with magnitudes as low as M_L 0.94 shows that the detection capabilities of the seismic stations, together with the data analysis methods used in this study, are capable of detecting events in proximity to seismic stations that are considerably weaker than the magnitude of completeness of the overall catalog. Considering the continuous monitoring that occurred for two years using four stations deployed around the Eavor-Lite™ closed-loop geothermal system and the final catalog that was generated, it is likely that no seismic events with a local magnitude of M_L 1 or larger occurred within, or near, the footprint of the EVR monitoring array.

This demonstrates that there is currently no evidence that the Eavor-Lite^{TM} closed-loop geothermal system induced any detectable seismic activity ($M_L > 1$) during the two-year monitoring period from November 1, 2020, to November 30, 2022. Furthermore, since the final catalog contained 94 events within the surrounding area in west-central Alberta – and the AER has enacted a nearby traffic-light protocol for induced seismicity – the overall region is demonstrably not seismically quiescent. This factor is important, as it refutes a potential counterargument that the apparent paucity of observed seismicity proximal to the Eavor-Lite^{TM} system could be dismissed simply because the region is non-seismogenic.

Conclusions

Alberta has recorded both natural seismicity (associated with ongoing far field tectonic processes relating to the Rocky Mountains) and induced seismicity relating to ongoing resource exploration (e.g. Li et al., 2022; Schultz et al., 2023). Seismicity associated with geothermal exploration has not been documented here but is still a concern to the regulator and the public, as it has been observed elsewhere in the world (e.g., Australia, Baisch, 2020; France, Fiori et al., 2023; North America, Koirala et al., 2024). In late 2019, Eavor Technologies Ltd. completed drilling and construction of a closed-loop geothermal pilot project in west-central Alberta. Local seismic monitoring of this project (the EVR array) began in November 2020 by the University of Calgary, with four broadband seismic stations within 10 km of the well site. Continuous seismic monitoring continued until November 2022, and combined with regional public seismic data, a compiled catalog of seismicity was generated during this time. Installation of the EVR array enhanced the detection capabilities of the regional monitoring stations in this area, and also added value with respect to monitoring ongoing geothermal operations at the closed-loop geothermal site.

Using a machine learning workflow, combined with event origin times from several other regional catalogs, a total of 94 seismic events were detected and located during the monitoring period. Among the detections we have identified quarry blasting, several felt natural events (e.g. the 14th February 2021, M_L 3.68 Banff event), as well as potentially induced seismicity within a cluster near Rocky Mountain House, Alberta, which appears to have been active for several decades. No events were detected within or close to the local monitoring array during the monitoring period (i.e., within a distance of 25 km). Due to limited far-field station distribution, the magnitude of completeness of the final compiled catalog is M_L2.24, although events below M_L 1.0 were recorded in areas of relatively dense station coverage. This suggests that the monitoring array close to the Eavor-Lite^{TM} closed-loop geothermal site had the capacity to monitor small magnitude events, the absence of which suggests no induced detectable seismicity occurred as a result of closed-loop geothermal operations at this site between November 2020 and November 2022.

Acknowledgements

This research was supported by funds from the Global Research Initiative (GRI) at the University of Calgary, which was supported by a grant from the Canada First Research Excellence Fund (CFREF). Eavor Technologies Inc. is thanked for funding to support the installation and operation of four seismic station in the EVR array reported in this study, as well as for many meaningful insightful conversations during this research. The authors would like to thank the Seismological Facility for the Advancement of Geoscience (SAGE) for hosting the public data and facilitating collaboration. Fault polygons and Leduc reef outlines shown in this report are use data provided by geoLOGIC Systems Ltd. © 2024. Figures 3, 6 and 7 were produced using PyGMT (https://www.pygmt.org/dev/index.html) and Figures 4, 5, 9 and 10 using Snuffler (https://pyrocko.org/docs/current/apps/snuffler/). The authors would like to thank Jeremy Gosselin for an insightful review of the manuscript.

Data Availability

The seismicity catalog developed for this study is available as Supplementary Data in both .csv and. quakeml format. The EVR station metadata and continuous miniseed data will be made openly available through the Seismological Facility for the Advancement of Geoscience (SAGE), after expiration of the embargo period (November 25, 2024) at https://doi.org/10.7914/SN/EO.

Author Contributions

Conceptualization: DWE; Fieldwork: KPM; Methodology: JRP, ROS, DWE, KPM; Formal Analysis: JRP, ROS, DWE; Visualization: KPM, ROS, JRP, DWE; Writing & editing: ROS, KPM,DWE, JRP. Originally involved in the study as a Postdoctoral researcher at the University of Calgary, author R. O. Salvage completed aspects of the seismic analysis reported herein during her present tenure as a Research Scientist at the Geological Survey of Canada.

References

Aki, K.(1965). Maximum likelihood estimate of b in the formula log n=a-bm and its confidence limits. *Bulletin of Earthquake Research, Institute Tokyo University*, *43*, p. 237-239.

Alberta Energy Regulator / Alberta Geological Survey (2023). Alberta Earthquakes Dashboard, https://ags-aer.shinyapps.io/Seismicity_waveform_app/, Last Accessed: 18 October 2024.

Alberta Geological Survey / Alberta Energy Regulator (2013). Regional Alberta Observatory for Earthquake Studies Network [Data set]: *International Federation of Digital Seismograph Networks*, https://doi.org/10.7914/SN/RV, Last Accessed: 8 August 2024.

Atkinson, G., Eaton, D. W., Ghofrani, H., Walker, D., Cheadle, B., Schultz, R., Shcherbakov, R., Tiampo, K., G., J., Harrington, R. M., Liu, Y., van der Baan, M., & Kao, H. (2016). Hydraulic fracturing and seismicity in the Western Canada Sedimentary Basin. *Seismological Research Letters, 87* (3), p. 631-647, https://doi.org/10.1785/0220150263.

Babaie-Mahani, A., & Kao, H. (2020). Determination of local magnitude for induced earthquakes in the Western Canada Sedimentary Basin: An update. *CSEG Recorder*, 45 (2), https://csegrecorder.com/articles/view/determination-of-local-magnitude-for-induced-earthquakes-in-the-wcsb.

Baisch, S. (2020)., Inferring In Situ hydraulic pressure from induced seismicity observations: An application to the Cooper Basin (Australia) geothermal reservoir. *Journal of Geophysical Research Solid Earth, 125* (8), e2019JB019070, https://doi.org/10.1029/2019JB019070

Baranova, V., Mustaqeem, A., & Bell, S. (1999). A model for induced seismicity caused by hydrocarbon production in the Western Canada Sedimentary Basin. *Canadian Journal of Earth Sciences*, 36 (1), 47-64, https://doi.org/10.1139/e98-080.

Beyreuther, M., Barsch, R., Krischer, L., Megies, T., Behr, Y., & Wassermann, J. (2010) ObsPy: A Python Toolbox for Seismology. *Seismological Research Letters*, 81 (3), 530-533, https://doi.org/10.1785/gssrl.81.3.530.

Brown, S. P. & Spang, J. H. (1978). Geometry and mechanical relationship of folds to thrust fault propagation using a minor thrust in the front ranges of the Canadian Rocky Mountains. *Bulletin of Canadian Petroleum Geology*, 26(4), 551-571, https://doi.org/10.35767/gscpgbull.26.4.551.

Candela, T., van der Veer, E. F., & Fokker, P. A. (2018). On the Importance of Thermo-elastic Stressing in Injection-Induced Earthquakes. *Rock Mechanics and Rock Engineering, 51* (12), 3925-3936, https://doi.org/10.1007/s00603-018-1619-6.

Chai, C., Maceira, M., Santos-Villalobos, H. J., Venkatakrishnan, S. V., Schoenball, M., Zhu, W., Beroza, G. C., & Thurber, C. (2020). Using a Deep Neural Network and Transfer Learning to Bridge Scales for Seismic Phase Picking. *Geophysical Research Letters, 47* (16), https://doi.org/10.1029/2020GL088651.

Eaton, D. W. & Eyre, T. S. (2018). Induced seismicity in western Canada: Causes and Consequences. *Geohazards 7*, Canmore 2018.

Eaton, D. W. (2018). Passive Seismic Monitoring of Induced Seismicity: Fundamental Principle and Application to Energy Technologies. *Cambridge University Press*, 2018, https://doi.org/10.1017/9781316535547.

Eavor (2020). Eavor-Lite Demonstration Project, https://eavor.com/about/technology. Last Accessed: 20 September 2020

Ester, M., Kriegel, H-P., Sander, J. & Xu, X. (1996). A density-based algorithm for discovering clusters in large spatial databases with noise. *KDD-96 Proceedings*, 226-231, https://cdn.aaai.org/KDD/1996/KDD96-037.pdf?source=post_page.

Fiori, R., Vergne, J., Schmittbuhl, J. & Zigone, D. (2023). Monitoring induced microseismicity in an urban context using very small seismic arrays: The case study of the Vendenheim EGS project. *Geophysics, 88* (5), https://doi.org/10.1190/geo2022-0620.1

Gabrielse, H., & Yorath, C. J. (1991). Geology of the Cordilleran Orogen in Canada. *Geological Survey of Canada, Geology of Canada Series, 4*, 844, https://doi.org/10.4095/134069.

Gutenberg, B., & Richter, C. F. (1956). Earthquake magnitude, intensity, energy, and acceleration: (Second Paper). *Bulletin of the Seismological Society of America, 46* (2), 105-145, https://doi.org/10.1785/BSSA0460020105.

Heinmann, S., Kriegerowski, M., Isken, M., Cesca, S., Daout, S., Grigoli, F., Juretzek, C., Megies, T., Nooshiri, N., Steinberg, A., Sudhaus, H., Vasyura-Bathke, H., Willey, T., & Dahm, T. (2017). Pyrocko – an open-source seismology toolbox and library, *GFZ Data Services,* https://doi.org/10.5880/GFZ.2.1.2017.001.

Horner, R., Barclay, J., & MacRae, J. (1994). Earthquakes and hydrocarbon production in the Fort St. John area of northeastern British Columbia. *Canadian Journal of Exploration Geophysics, 30* (1), 39-50, https://cseg.ca/wp-content/uploads/1994_06_quakes_hydrocarb_prod.pdf.

Hui, G., Chen, S., Gu, F., Pang, Y., Yu, X., & Zhang, L. (2021). Insights on Controlling Factors of Hydraulically Induced Seismicity in the Duvernay East Shale Basin. *Geochemistry Geophysics Geosystems, 22* (2), e2020GC009563, https://doi.org/10.1029/2020GC009563.

Koirala, R., Kwiatek, G., Shirzaei, M., Brodsky, E., Cladouhos, T., Swyer, M., & Goebel, T. (2024). Induced seismicity and surface deformation associated with long-term and abrupt geothermal operations in Blue Mountain, Nevada. *Earth and Planetary Science Letters, 643,* 118883, https://doi.org/10.1016/j.epsl.2024.118883.

Krischer, L., Megies, T., Barsch, R., Beyreuther, M., Lecocq, T., Caudron, C., &Wassermann, J. (2015). ObsPy: a bridge for seismology into the scientific Python ecosystem. *Computational Science & Discovery*, *8*(1), https://doi.org/10.1088/1749-4699/8/1/014003.

Lamontagne, M., Halchuk, S., Cassidy, J. F., & Rogers, G. C. (2008). Significant Canadian Earthquakes of the Period 1600-2006. *Seismological Research Letters, 79* (2), 211-223, https://doi.org/10.1785/gssrl.79.2.211.

Li, T., Gu, J., Wang, J., Wang, R., Yusifbayov, J., Reyes Canales, M., & Shipman, T. (2022). Earthquakes Induced by Wastewater Disposal near Musreau Lake, Alberta, 2018-2020. *Seismological Research Letters, 93* (2A), 727-728, https://doi.org/10.1785/0220210139.

Li, J., Rojas-Parra, J., Salvage, R. O., Eaton, D. W., Innanen, K. A., Yu, Y. G., & Sun, W. (2024). Machine learning aids rapid assessment of aftershocks: Application to the 2022-2023 Peace River earthquake sequence, Alberta, Canada. *The Seismic Record,* 4(1), 21-31, https://doi.org/10.1785/0320230051.

Lomax, A., Michelini, A., & Curtis, A. (2014). Earthquake location, Direct, Global-Search Methods: *In: Meyers, R., (eds) Encyclopedia of Complexity and System Science,* Springer, New York, NY. https://doi.org/10.1007/978-3-642-27737-5_150-2.

Lomax, A., Virieux, J., Volant, P., & Berge-Thierry, C. (2000). Probabilistic Earthquake Location in 3D and Layered Models, *Springer Netherlands*, 101-134.

Marion, K. P., Eaton, D. W., & Salvage, R. O. (2023). Rethinking historical models of induced seismicity in Rocky Mountain House, Alberta, Canada: Is brine disposal to blame? *XXVIII General Assembly of the International Union of Geodesy and Geophysics (IUGG)*, Berlin 2023.

Milne, W. G., Rogers, G. C., Riddihough, R. P., McMechan, G. A., & Hyndman, R. D. (1978). Seismicity of western Canada. *Canadian Journal of Earth Sciences, 15* (7), 1170-1191, https://doi.org/10.1139/e78-123.

Nanometrics Inc. (2012). Apollo Project Version 2.3 User Guide, *Technical Report no. 16106R8*, Nanometrics Inc., Kanata, Ontario, Canada

Natural Resources Canada (2015). 2015 National Building Code of Canada seismic hazard maps, Available at: https://www.earthquakescanada.nrcan.gc.ca/hazard-alea/zoning-zonage/NBCC2015maps-en.php, Last accessed: 22 March 2024.

Natural Resources Canada (2019). Earthquake Details (2019-03-04), available at: https://www.earthquakescanada.nrcan.gc.ca/recent/2019/20190304.1255/index-en.php, last accessed: 8 August 2024.

Natural Resources Canada (2021a). Earthquake Details (2021-10-20), available at: https://www.earthquakescanada.nrcan.gc.ca/recent/2021/20211021.0323/index-en.php, last accessed: 22 March 2024.

Natural Resources Canada (2021b). Earthquake Details (2021-02-13), available at: https://www.earthquakescanada.nrcan.gc.ca/recent/2021/20210214.0133/index-en.php, last accessed: 22 March 2024.

Perkins, T. K., & Gonzalez, J. A. (1985). The Effect of Thermoelastic Stresses on Injection Well Fracturing. *Society of Petroleum Engineers Journal, 25*(), 78-88, https://doi.org/10.2118/11332-PA.

Rebollar, C. J., Kanasewich, E. R., & Nyland, E. (1982). Source parameters from shallow events in the Rocky Mountain House earthquake swarm. *Canadian Journal of Earth Sciences, 19* (5), 907-918, https://doi.org/10.1139/e82-076.

Rebollar, C. J., Kanasewich, E. R., & Nyland, E. (1984). Focal depths and source parameters of the Rocky Mountain House earthquake swarm from digital data at Edmonton. *Canadian Journal of Earth Sciences, 21* (10), 1105-1113, https://doi.org/10.1139/e84-115.

Reiter, K., & Heidbach, O. (2014). 3-D geomechanical–numerical model of the contemporary crustal stress state in the Alberta Basin (Canada). *Solid Earth, 5* (2), 1123-1149, https://doi.org/10.5194/se-5-1123-2014.

Rivard, C., Lavoie, D., Lefebvre, R., Sejourne, S., Lamontagne, C., & Duchesne, M. (2014). An overview of Canadian shale gas production and environmental concerns. *International Journal of Coal Geology, 126*, 64-76, https://doi.org/10.1016/j.coal.2013.12.004.

Ross, G. M., Parrish, R. R., Villeneuve, M. E., & Bowring, S. A. (1991). Geophysics and geochronology of the crystalline basement of the Alberta Basin, western Canada. *Canadian Journal of Earth Sciences, 28* (4), 512-522, https://doi.org/10.1139/e91-045.

Salvage, R. O., Eaton, D. W., Furlong, C. M., Dettmer, J. & Pedersen, P. (2024). Induced or Natural? Towards rapid expert assessment, with application to the Mw 5.2 Peace River Earthquake Sequence. *Seismological Research Letters, 95* (2A), p. 758-772, https://doi.org/10.1785/0220230289.

Schubert, E., Sander, J., Ester, M., Krigel, H. P. & Xu, X. (2017). DBSCAN revisited: Why and how you should (still) use DBSCAN, *ACM Transactions on Database Systems (TODS), 42*(3), 1-19, https://doi.org/10.1145/3068335

Schultz, R., Corlett, H., Haug, K., Kocon, K., MacCormack, K., Stern, V., & Shipman, T. (2016) Linking fossil reefs with earthquakes: Geologic insight to where induced seismicity occurs in Alberta. *Geophysical Research Letters, 46* (6), 2534-2542, https://doi.org/10.1002/2015GL067514

Schultz, R., Wang, R., Gu, Y. G., Haug, K., & Atkinson, G. (2017). A seismological overview of the induced earthquakes in the Duvernay play near Fox Creek, Alberta. *Journal of Geophysical Research: Solid Earth, 122*, 492-505, https://doi.org/10.1002/2016JB013570.

Schultz, R., & Stern, V. (2015). The Regional Alberta Observatory for Earthquake Studies Network (RAVEN). *CSEG Recorder, 40*(8), https://csegrecorder.com/assets/pdfs/2015/2015-10-RECORDER-AB_Observatory_for_Earthquakes.pdf.

Schultz, R., Woo, J.-U., Pepin, K., Ellsworth, W. L., Zebkar, H., Segall, P., Gu, Y. J., & Samsonov, S. (2023). Disposal from In Situ Bitumen Recovery Induced the M_L 5.6 Peace River Earthquake. *Geophysical Research Letters, 50* (6), e2023GL102940, https://doi.org/10.1029/2023GL102940.

Shen, L. W., Schmitt, D. R., Wang, R., & Hauck, T. E. (2021). States of In Situ Stress in the Duvernay East Shale Basin and Willesden Green of Alberta, Canada: Variable In Situ Stress States Effect Fault Stability. *Journal of Geophysical Research: Solid Earth, 126*(6), https://doi.org/10.1029/2020JB021221.

Stern, V. H., Schultz, R., Shen, L., Gu, Y., & Eaton, D. W. (2013). Alberta earthquake catalogue, version 1.0: September 2006 through December 2010. Alberta Energy Regulator, AER/AGS Open File Report, 2013-15, 29 p., https://static.ags.aer.ca/files/document/OFR/OFR_2013_15.pdf.

Thorson, A. Atchley, S., Weissenberger, J., Yeates, D., & Rau, E. (2019). Stratigraphic Partitioning and Distribution of Reservoir Attributes Within the Late Devonian Duvernay Formation, Western Canada Sedimentary Basin. *SPE/AAPG/SEG Unconventional Resources Technology Conference*, Denver, Colorado, USA.

Toews, M., & Holmes, M. (2021). Eavor-Lite Performance Update and Extrapolation to Commercial Projects. GRC Transactions, 45, https://www.eavor.com/wp-content/uploads/2021/11/Eavor-Lite-Performance-Update-and-Extrapolation-to-Commercial-Projects.pdf.

Toews, M., Riddell, D., Vany, J., & Schwarz, B. (2020). Case Study of a Multilateral Closed-Loop Geothermal System. *Proceedings World Geothermal Congress 2020*, Reykjavik, Iceland, April 26 – May 2, 2020, https://www.eavor.com/wp-content/uploads/2022/04/31065-Matthew-Toews-WGC-2020.pdf.

Trnkoczy, A. (2009). Understanding and parameter setting of STA/LTA trigger algorithm. *New Manual of Seismological Observatory Practice (NMSOP)*, Deutsches GeoForschungsZentrum GFZ, p. 1-20, https://gfzpublic.gfz-potsdam.de/rest/items/item_4097/component/file_4098/content.

Vany, J., Hirschmiller, J., & Toews, M. (2020). Subsurface characterization methods for multilateral closed loop geothermal systems. Case study of field scale technology demonstration project in Alberta, Canada: GRC Transactions, 44, 1360-1361, https://www.eavor.com/wp-content/uploads/2022/04/Vany-et-al-Draft-Eavor-Lite-Paper-March-19.pdf.

Vasyura-Bathke, H., Dettmer, J., Biegel, K., Salvage, R. O., Eaton, D., Ackerley, N., Samsonov, S., & Dahm, T. (2023). Bayesian inference elucidates fault-system anatomy and resurgent earthquakes induced by continuing saltwater disposal. *Communications Earth & Environment, 4,* 407, https://doi.org/10.1038/s43247-023-01064-1.

Wang, J., Li, T., Gu, Y. J., Schultz, R., Yusifbayov, J., & Zhang, M. (2020). Sequential Fault Reactivation and Secondary Triggering in the March 2019 Red Deer Induced Earthquake Swarm. *Geophysical Research Letters,47* (22), https://doi.org/10.1029/2020GL090219.

Wang, R., Gu, Y. J., Schultz, R., Kim, A., & Atkinson, G. (2016). Source analysis of potential hydraulic-fracturing-induced earthquake near Fox Creek, Alberta. *Geophysical Research Letters, 43* (2), https://doi.org/10.1002/2015GL066917.

Wiemer, S., & Wyss, M. (2000). Minimum magnitude of completeness in earthquake catalogs: Examples from Alaska, the western United States, and Japan. *Bulletin of the Seismological Society of America, 90*(4), 859–869, https://doi.org/10.1785/0119990114.

Wetmiller, R. J. (1986). Earthquakes near Rocky Mountain House, Alberta, and their relationship to gas production facilities. *Canadian Journal of Earth Sciences, 23* (2), 172-181, https://doi.org/10.1139/e86-020.

Zhu, W., & Beroza, G. C. (2018). PhaseNet: a deep-neural-network-based seismic arrival-time picking method. *Geophysical Journal International, 216*(1), 261-273, https://doi.org/10.1093/gji/ggy423.

Zhu, W., McBrearty, I. W., Mousavi, S. M., Ellsworth, W. L., & Beroza, G. C. (2022). Earthquake Phase Association Using a Bayesian Gaussian Mixture Model. *Journal of Geophysical Research: Solid Earth, 127* (5), https://doi.org/10.1029/2021JB023249.

Table S1: Metadata for the EVR stations installed for this study.

Network	Station	Latitude	Longitude	Elevation (m)	Depth (m)	H1 Azimuth (deg)	Sensor Type	Channels	Sampling rate (Hz)	Sensitivity V/(m/s)
EO	EVR1	52.27795	-114.547761	1006	0.46	356	Trillium Compact	3	100	749.1
EO	EVR2	52.23869	-114.531498	1000	0.46	350	Trillium Compact	3	100	749.1
EO	EVR3	52.21475	-114.604649	989	0.30	352	Trillium 240	3	100	1168.2
EO	EVR4	52.25307	-114.608431	998	0.46	354	Trillium Compact PH	3	100	749.1

Table S2: Parameters varied within GaMMA that were used to generate different provisional earthquake catalogs. Combining events identified in each iteration and removing duplicates resulted in an initial catalog of 230 events..

Iteration	Vp [km/s]	Vs [km/s]	dbscan_eps [s]	Oversampling factor	Max_sigma1	# of potential detected events
fast	6.26	3.61	29.23	8	10	152
mid	6.08	3.49	29.00	8	15	176
slow	5.77	3.27	30.00	8	10	147
oversample	6.08	3.49	30.09	10	2.5	159
initial_points	6.08	3.49	30.09	8	10	161

Table S3: NLL input parameters – see https://github.com/alomax/NonLinLoc for more information on parameters.

Control	Command	Parameter	Value
Vel2Grid	VGGRID	xNum, yNum	1000
		zNum	100
		xOrig, yOrig	-700.0
		zOrig	0.0
		dx, dy, dz	1.0
		gridType	SLOW_LEN
Grid2Time	GTMODE	gridMode	GRID3D
		angleMode	ANGLES_YES
Time2EQ	EQMODE		SRCE_TO_STA
	EQVPVS		1.76
	EQQUAL2ERR		0.05 0.1 0.5 1.0 99999.9
NLLoc	LOCHYPOUT		SAVE_NLLOC_SUM
	LOCSEARCH	Type	OCT
		initNumCells_x,	30
		initNumCells_z	3
		minNodeSize	0.01
		MaxNumNodes	300000
		NumScatter	5000
		useStationDensity	0
		stopOnMinNodeSize	1
	LOCGRID	xNum, yNum	600
		zNum	12
		xOrig, yOrig	-300.0
		zOrig	0.0
		dx, dy, dz	1.0
		gridType	PROB_DENSITY
		saveFlag	SAVE
	LOCMETH	Method	EDT_OT_WT
		maxDistStaGrid	405.0
		minNumberPhases	4
		maxNumberPhases	-1
		minNumberSphases	-1
		VpVsRatio	-1
		maxNum3dGridMemory	6
		minDistStaGrid	-1.0
		iRejectDuplicateArrivals	1
	LOCGAU		0.2 0.0
	LOCGAU2		0.02 0.05 0.2
	LOCPHASEID	P	P p
		S	S s
	LOCQUAL2ERR		0.1 0.5 1.0 2.0 99999.9
	LOCANGLES	ANGLES_YES	5
	LOCPHSTAT	RMS_Max	9999.0
		NRdgs_Min	-1
		Gap_Max	9999.0
		P_ResidualMax	1.0
		S_ResidualMax	1.0
		Ell_Len3_Max	20.0
		Hypo_Depth_Min	-20.0
		Hypo_Depth_Max	9999.9
		Hypo_Dist_Max	9999.9

Figure S1: A) The metal enclosure for EVR3 in Fall 2020. The Taurus digitizer unit sits inside the housing, while the seismograph itself is buried at ~0.5 m depth, beneath the soil. B) The seismometer at EVR4 during decommissioning in August 2023 alongside some of the seismometer housing; despite water getting into the housing for the Taurus digitizer, the equipment remained undamaged. Photos courtesy of K.P. Marion.

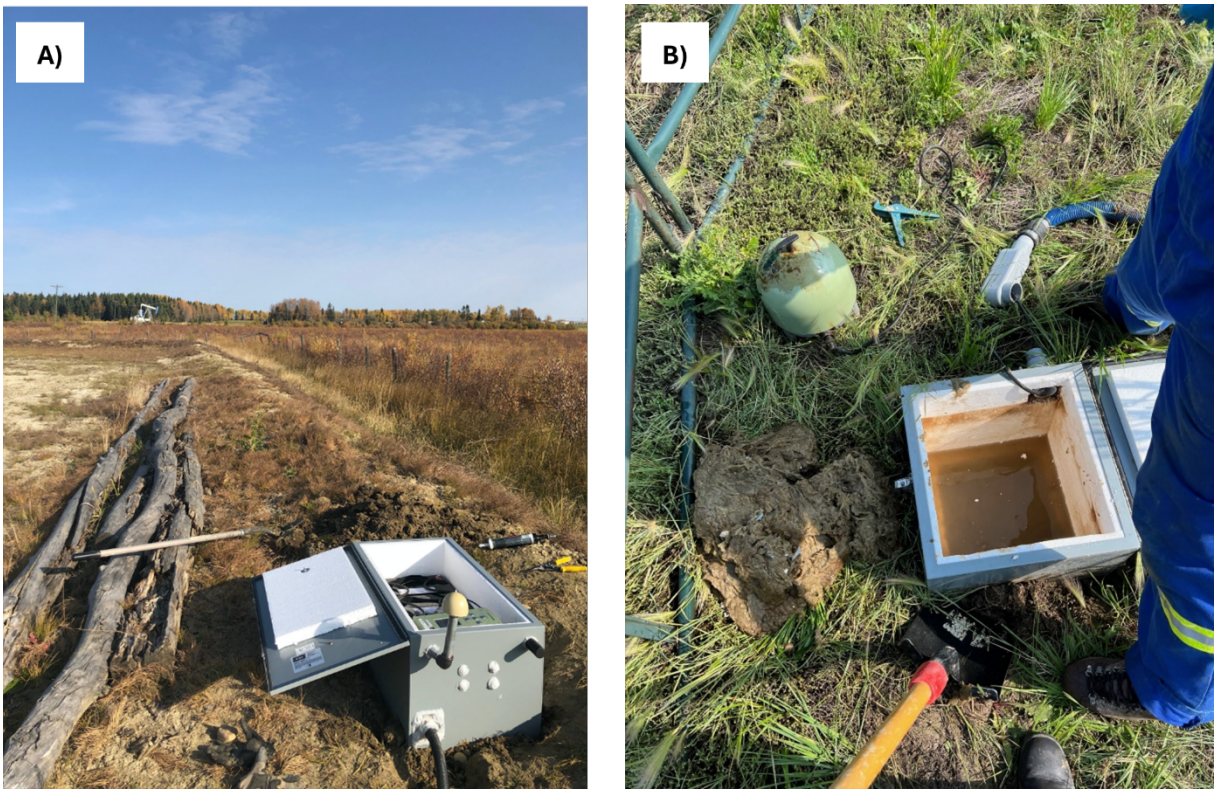

Electronic Supplements

OFR_EVR_catalog.csv

OFR_EVR_catalog.csv contains a .csv file with the 94 detected seismic events determined by this machine learning workflow. Column headings are as follows:

- *time:* Origin time of detected event in UTC.
- *longitude*: Calculated longitude of event using NonLinLoc software (Lomax et al., 2009), in degrees.
- *Latitude:* Calculated latitude of event using NonLinLoc software (Lomax et al., 2009), in degrees.
- *depth_km:* Calculated depth of event using NonLinLoc software (Lomax et al., 2009), in kilometers.
- *ML:* Local magnitude calculated using the formula of Babaie-Mahani and Kao (2020), with the correction factor of 0.79 added.
- *standard_error_x_km:* Standard error in x direction in kilometers calculated using covariance value of the probability density function (Lomax et al., 2009).
- *Standard_error_y_km:* Standard error in y direction in kilometers calculated using covariance value of the probability density function (Lomax et al., 2009).
- *Standard_error_z_km:* Standard error in z direction (depth) in kilometers calculated using covariance value of the probability density function (Lomax et al., 2009).
- *ML_error_max:* Maximum error in calculated magnitude between ML (column 5 of .csv) and calculated ML at all other stations with picks, in local magnitude units.
- *ML_error_mean:* Mean error in calculated magnitude between ML (column 5 of .csv) and calculated ML at all other stations with picks, in local magnitude units.

OFR_EVR_catalog.xml

OFR_EVR_catalog.xml contains a .xml (QuakeML format) catalog with the 94 detected seismic events determined by this machine learning workflow. For each event in the catalog, information relating to phase picks on each channel and station, as well as the calculated latitude, longitude and depth of the event using the NonLinLoc software (Lomax et al., 2009), and the magnitude calculated using the Babaie-Mahani and Kao (2020) formula with an added constant of 0.79 for comparison to the AER catalog, is provided.

`